Institut für Computergraphik und Algorithmen
Technische Universität Wien
Karlsplatz 13/186/2
A-1040 Wien
AUSTRIA
Tel: +43 (1) 58801-18601
Fax: +43 (1) 58801-18698

Institute of Computer Graphics and Algorithms
Vienna University of Technology
email:
technical-report@cg.tuwien.ac.at
other services:
http://www.cg.tuwien.ac.at/
ftp://ftp.cg.tuwien.ac.at/

TECHNICAL REPORT

Surface Extraction from Multi-Material Components for Metrology using Dual Energy CT

Christoph Heinzl
Vienna University of Technology, Institute of Computer Graphics and Algorithms
Johann Kastner
Upper Austrian University of Applied Sciences, Wels Campus
Eduard Gröller
Vienna University of Technology, Institute of Computer Graphics and Algorithms

TR-186-2-07-06
May 2007

Keywords: DECT image fusion, local surface extraction, Dual Energy CT, metrology, dimensional measurement, variance comparison.

Surface Extraction from Multi-Material Components for Metrology using Dual Energy CT

Christoph Heinzl*
Vienna University of Technology, Institute of Computer Graphics and Algorithms

Johann Kastner†
Upper Austrian University of Applied Sciences, Wels Campus

Eduard Gröller‡
Vienna University of Technology, Institute of Computer Graphics and Algorithms

May 9, 2007

Abstract

This paper describes a novel method for creating surface models of multi-material components using dual energy computed tomography (DECT). Application scenario for the presented work is metrology and dimensional measurement of multi-material components in industrial high resolution 3D X-Ray computed tomography (3DCT). The basis of this method is the dual source / dual exposure technology using the different X-Ray imaging modalities of a high precision micro-focus and a high energy macro-focus X-Ray source.

The presented work aims at combining the advantages of both X-Ray modalities in order to facilitate dimensional measurement of multi-material components with high density material within low density material. We propose a pipeline model using image fusion and local surface extraction technologies: A prefiltering step reduces data inherent noise. For image fusion purposes the datasets have to be registered to each other. In the fusion step the benefits of each modality are combined. So the structure of the specimen is taken from the low precision, blurry, high energy dataset while the sharp edges are adopted and fused into the resulting image from the high precision, crisp, low energy dataset. In the final step a reliable surface model is calculated of the fused dataset, which locally adapts the surface model by moving surface vertices in the direction of the corresponding point normal to a position with maximum gradient magnitude.

The major contribution of this paper is the development of a specific workflow for dimensional measurement of multi-material industrial components from high resolution industrial CT data. Several algorithms are extended to take two data sources with complementary strengths and weaknesses into account. The presented workflow is crucial for the following visual inspection of deviations.

*e-mail: c.heinzl@fh-wels.at
†e-mail: j.kastner@fh-wels.at
‡e-mail: groeller@cg.tuwien.ac.at

1 Introduction

In state-of-the-art engineering the demands concerning functionality of industrial components continuously increases the complexity of new parts. But not only the functionality is rising. Also the demands in terms of weight reduction, increased stability and in terms of new materials (e.g. carbon fibre reinforced plastics) force constructors to design new function oriented and complex parts. In order to meet the requirements and specifications of construction drawings, the manufacturing quality has to be assured using top of the line quality assurance modalities. Metrology (from Greek *metron* (measure), and *-logy*) is defined as the science of measurement. Metrology includes all theoretical and practical aspects of measurement [25]. In quality assurance, metrology is a very common modality which measures the surface geometry of a component, e.g. distances, wall-thicknesses or diameters. Usually this is accomplished by means of coordinate measurements using tactile or optical sensors. This technology allows to calculate surface dimensions at a calibrated measurement precision over a defined measurement area.

In recent years the methodologies of metrology and dimensional measurement were expanded introducing the novel technology of industrial 3D X-Ray computed tomography (3DCT). 3DCT is an established method for

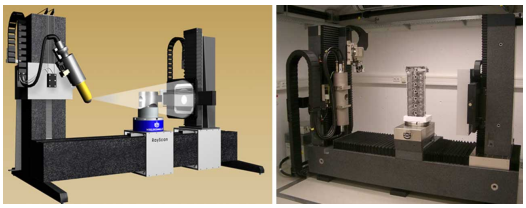

Figure 1: 3D X-Ray computed tomography system at the Upper Austria University of Applied Sciences - Wels Campus. General design of the CT: Left: granite pillar with 225 keV and 450 keV X-Ray sources. Center: rotary plate. Right: granite pillar with amorph silicon matrix detector. A single 360 degree turn is sufficient to acquire the full geometry of a specimen.

visualization and non-destructive-testing (NDT) of industrial components [5]. More recently 3DCT gained importance in the area of dimensional measurement of industrial components. Figure 1 shows the principle scheme and a photograph of the 3DCT of the Upper Austrian University of Applies Sciences - Wels Campus. A series of X-Ray attenuation measurements is generated, which is used to produce a 3D grid of greyvalues corresponding to the spatial density distribution [10]. The special capabilities of 3DCT provide full geometric information of a specimen including inner and hidden structures. So using a single scan, a specimen is characterized concerning material defects and geometrical irregularities of the manufacturing process without destroying the specimen. Furthermore, using 3DCT typical limitations of tactile and optical coordinate measurement technology can be avoided (e.g. deformable surfaces and reflecting glass probes).

The major disadvantage of industrial CT compared to medical CT is: Medical CTs produce calibrated and less artefacts affected datasets using collimated, highly sensitive line detectors. As industrial 3DCTs with cone beam geometry and flat panel detectors are prone to artefacts like noise-induced streaks, aliasing, beam-hardening, partial volume or scattered radiation effects [4], the quality of the datasets is easily affected by the environmental conditions of the measurement. Some of the parameters which have a major contribution to the dataset's quality are: the specimen's geometry, the penetration lengths, the positioning of the specimen in the ray, the measurement parameters and the specimen's material combination.

Especially when scanning multi-material specimens with high differences in density and therefore attenuation coefficient of the materials, severe streaking artefacts prevent from dimensional measuring. Usually, technicians in measurement technology disassemble the multi-material components. Each material is measured in a separate scan using optimal X-Ray parameters. This procedure is time consuming. The specimen has to be disassembled and is in several cases destroyed. In the special case of a pressure sensor from automotive industry, the sensor is cast integral into the plastic body and can not be removed without destroying the specimen. For common single-material industrial components, the workflow for dimensional measuring can be summed up as follows: A prefiltering step reduces the reconstructed dataset's inherent noise in order to support surface detection. For common surface extraction tasks in industrial applications, usually a single isovalue is specified to distinguish between material and air [23]. A polygonal mesh is extracted along the selected isovalue using a surface creation algorithm. For example the marching cubes algorithm creates triangle models of constant density surfaces from 3D volume data [12]. Finally the geometry of an extracted surface model is compared to the specifications of the computer aided design (CAD) model using variance comparison. The corresponding deviations between the reference and the test model are calculated and visualized by color-coding scalar deviations on the surface of the reference model.

Multi-material components with high density differences are not suitable for the common workflow of dimensional measurement using 3DCT. High density and highly absorbing materials (e.g. steel) produce scattered radiation which is manifested in the reconstructed dataset. So the low absorbing material is simply covered by the different characteristics of artefacts from the strong absorbing material. If a global thresholding method for surface extraction was applied on an artefact affected dataset, holes and artificial structures introduced by different artefact types modify the surface models. So a reliable dimensional measurement is in most cases impossible. In Figure 2 these circumstances are depicted.

To improve measurement results, recent research activities try to exploit Dual Energy Computed Tomography (DECT). By tomographing a specimen using different energies and therefore different energy spectras of the X-Ray source, it is possible to combine information of both reconstructions in order to quantify the different materials of a component.

This paper concentrates on designing a new workflow to facilitate dimensional measurements of multi-material components. The reconstructed datasets of both measurement modalities are adaptively fused on a regional basis and a valid surface model for dimensional measurement is locally determined. The major goal of our

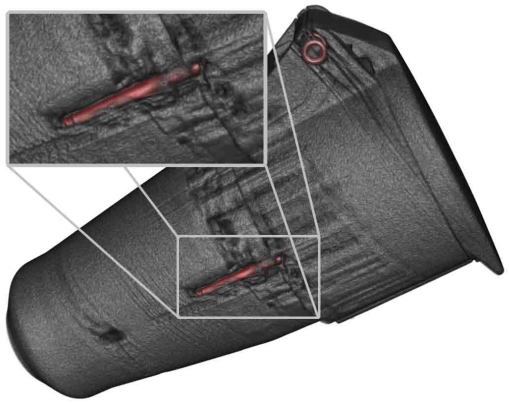

Figure 2: Scattered radiation, beam hardening, and other physical effects produce severe artefacts, which modify the dataset and prevent a reliable global isosurface extraction. Artefacts manifest themselves as holes and artificial stuctures. Note: the specimen's orientation in the beam is clearly determined by the artefact's characteristic. In the rendering even a hidden screw from inside the specimen appears (high density objects are depicted in red).

work is to design the DECT workflow to follow typical dimensional measurement constraints. The method has to be applicable for typical dimensional measurement tasks and has to be practicable in terms of quality and data-processing speed. The greyvalues of the two scans are taken as ground truth, assuming no additional information of CAD models or additional specifications of primives, e.g. cylinders, cuboids, in the scanned data. The special setup of the industrial 3DCT at the Upper Austrian University of Applied Sciences - Wels Campus is used to facilitate bimodal DECT scans. In this setup a dual X-Ray source design was realized using a 450 kV macro focus tube for the high energy scans and a 250 kV micro focus tube for the high precision measurements.

2 Related work

2.1 Dual energy computed tomography

Concerning data acquisition in DECT there are two different techniques: the dual exposure / dual source and the dual (layer) detector technique [19]. Using the dual exposure / dual source technique a specimen is measured twice using different X-Ray energies. Usually a high energetic measurement and a low energetic measurement are carried out successively without moving the specimen on the rotary plate. In order to combine both measurements either the position of the specimen may not be changed between the measurements or an accurate registration of the datasets has to be performed. A major disadvantage of the dual exposure / dual source technique is twice the measurement time which is needed to tomograph a specimen and also twice the data capacity is needed to store the data. The dual exposure / dual source method is already used in the area of medical CT to characterize material-specific differences in attenuation for classification of tissue types [21]. In the area of industrial CT this method constitutes a novel enhancement for applications, which is usable on a widespread variety of existing 3DCTs.

Using a dual detector technique only a single measurement of the specimen is necessary. A modified detector consisting of two separate layers generates two penetration images: the front layer detects low energy photons and the back layer high energy photons. The disadvantage of this method is that the energy separation of these detectors is rather poor [19]. An application area of this technique is baggage control systems for airport security [7]. Especially in this area, it is essential to classify materials with similar density in order to distinguish pieces of baggage of being either dangerous or safe. Another application area of the dual detector technique is the examination of drilling cores concerning material properties [8]. Transferring the principle of the dual detector technique to industrial CT is not as easy, because modified detectors have to be installed and the data acquisition software has to be adapted.

Due to specifications of our 3DCT equipment the dual exposure / dual source technique was used for our DECT measurements.

2.2 Image Fusion

The general aim of image fusion is to combine a set of input images into a single output image which preserves the salient information from each input image, suppresses noise and irrelevant parts of input images, and does not generate distortions, artefacts, or inconsistencies in the fused output [11]. Generally image fusion algorithms can be grouped into the following categories [15]:

In Arithmetic image fusion the resulting image is calculated by multiplying a weight factor with each dataset. In the second step the datasets are combined through voxelwise addition of the weighted data. Arithmetic image fusion is an efficient, easy to use image fusion method, which may be further improved by concentrating on certain areas of interest.

Color space fusion tries to make use of the human vision system. According to the the human vision system the data is separated into color channels. The problem of this approach is to create meaningful mappings from the input to a color channel in order to improve data [15]. As usually 3DCT data is stored in monochrome greyvalues this method is not applicable in the presented application area.

Multi-scale image fusion methods decompose input data into a multi-resolution image pyramid with a predefined number of layers. The image pyramids are combined starting at the coarsest layer by fusing corresponding images. After fusion the image pyramid is reconstructed to the final image. As image decomposition and reconstruction especially of large high resolution 3DCT datasets are time and memory consuming, multi-scale image fusion is not the method of choice for our application scenario.

The fourth category integrates neural networks, statistical a priori models, and optimization based approaches.

In the proposed DECT workflow an adapted version of the weighted arithmetic image fusion is used. It employs a region based encoding of the weights for each of the two datasets.

2.3 Local surface extraction

There are several methods in the area of industrial 3DCT that try to improve on surface extraction of industrial 3DCT data. Generally they can be grouped in two categories: the dataset is enhanced by artefact reduction [9] in order to generate a dataset with homogeneous greyvalues for each material. In this case, a single threshold is sufficient.

Techniques in the second category extract the best possible surface of the underlying data. Steinbeiss [22] developed algorithms, which locally adapt surface vertices to determine the best local surface position. Using an initial suitable surface model of the specimen, greyvalue profiles are calculated in the direction of each point's surface normal. The vertex location is then adjusted to correspond to the position with maximal gradient magnitude. Whitaker et al. [24] introduced an approach that directly operates on voxel data. In this approach the intermediate step of converting data to another representation is not necessary. The basic idea is to consider the zero level-set of a volume as a deformable surface. The surface is then deformed in order to minimize the mean curvature on the surface. Bischoff and Kobbelt [1] introduced algorithms on isosurface topology simplification and isosurface reconstruction with topology control. They use a priori knowledge about the topology of the input data to eliminate topological artefacts which is not available in our special application scenario. A method, which extracts a surface model from binary data was proposed by Gibson [2]. This method produces feature-preserving surface models by using a relaxation scheme within predefined constraints. In a large part the quality of this method depends on the prior segmentation. Heinzl et al. [3] proposed a pipeline model which uses common 3D image processing filters for preprocessing and segmentation of 3DCT datasets in order to create the surface model. In particular, a pre-filtering step reduces noise and artefacts without blurring edges in the dataset. A watershed filter is applied on the gradient information of the smoothed data to create a binary dataset. Finally the surface model is constructed, using constrained elastic-surface nets to generate a smooth but feature preserving mesh. For local surface extraction a modified version of Steinbeisses algorithm [22] is applied, which uses a modified noise reduction scheme.

In the following section the DECT workflow for surface extraction from multi-material components is introduced and covered in detail. Further more the results are discussed when applying the workflow on testparts as well as on real world industrial components.

3 DECT workflow for surface extraction from multi-material components

The basis of our approach is the dual source / dual exposure technology using a micro-focus and a macro-focus X-Ray source. The high energetic (HE) macro-focus CT scan generates a nearly artefact-free but blurry, less precise and more noisy data. Usually macro-focus CT is the method of choice when examining large and high density components. However, the disadvantage of this method is that due to the higher used energies of macro-focus X-Ray sources, the X-Ray spot size (origin of the X-Rays) is larger compared to micro-focus X-Ray sources. It is approximately 2 mm versus 7 μm to 320 μm depending on the selected energy setting. So the ideal case of a near punctiform X-Ray source for an optimal projection image on the detector is abandoned in macro-focus CT in order to achieve higher penetration lengths. In contrast, the low-energetic (LE) micro-focus measurement generates high precision but artefact affected data. The smaller X-Ray spot size supports in the generation of crisp and precise images, but the limited energy restricts penetration lengths.

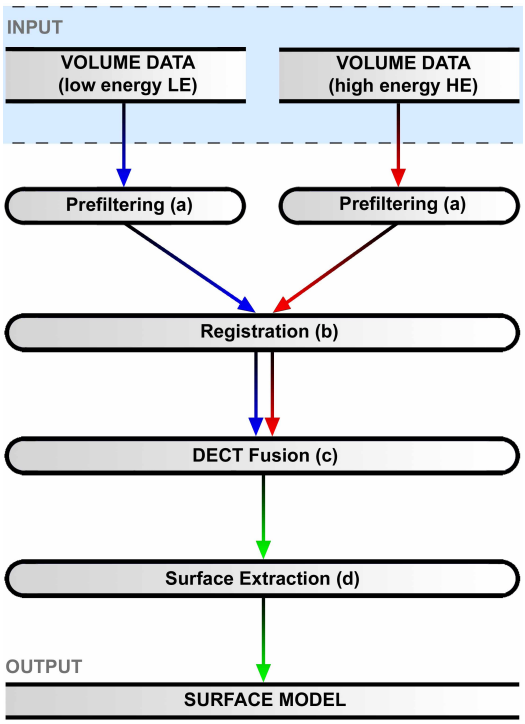

Figure 3: DECT workflow for surface extraction from multi-material components; Input1: Volume dataset of low energetic CT scan, Input2: Volume dataset of high energetic CT scan; Output: Improved surface mesh.

In the previous section most of the approaches mentioned are focused on a specific problem within the visualization pipeline. Our goal was to combine and extend existing methods according to the requirements of metrology in order to create a workflow, which is applicable in every day use for dimensional measurement of multi-material components. In the following subsections all components of the proposed DECT workflow including DECT fusion and local surface extraction are discussed in detail (see Figure 3).

3.1 Preprocessing

Due to different imaging modalities and different signal to noise ratios in each of the two measurements, a preprocessing step is essential. Both high energy (HE) and low energy (LE) datasets are affected to a certain degree by ambient noise. Because of a more intense noise level of the detector in the higher energy bands, especially the HE dataset has to be preprocessed to reduce noise and smaller artefacts. This is accomplished by applying anisotropic diffusion. Compared to isotropic smoothing, the characteristic of anisotropic diffusion filters is to smooth the data without blurring or moving edges which is unacceptable in the area of metrology and dimensional measurement. Anisotropic-diffusion methods are used to reduce noise in images while preserving specific image features [17]. Perona and Malik's method calculates multi-scale descriptions of images. If an image $U(\mathbf{x})$ is embedded in a higher dimensional function of derived images $U(\mathbf{x},t)$ then this higher dimensional function represents the solution of the heat diffusion equation,

$$\frac{dU(\mathbf{x},t)}{dt} = \nabla \cdot C \nabla U(\mathbf{x},t) \tag{1}$$

which is constrained by a constant conductance coefficient C and the initial condition $U(\mathbf{x},0) = U(\mathbf{x})$ representing the original image. If C is extended to a function of $\mathbf{x}$, the solution of the heat equation will be

$$\frac{dU(\mathbf{x},t)}{dt} = C(\mathbf{x})\Delta U(\mathbf{x},t) + \nabla C(\mathbf{x}) \nabla U(\mathbf{x},t) \tag{2}$$

A variable conductance term C can now modify the way the diffusion process takes place. Typically, C is chosen as a function of image features. This allows to selectively preserve or remove features by anisotropically varying the diffusion strength. Specifying C as a non-negative monotonically descending function as in

$$C(\mathbf{x}) = e^{-\left(\frac{\|\nabla U(\mathbf{x})\|}{K}\right)^2}, \qquad K = const \tag{3}$$

will force the diffusion to mainly take place in homogeneous interior regions. It will not affect the boundary regions [6]. When applying an anisotropic-diffusion filter, the dataset's inherent noise can be significantly reduced without loosing edge information. Scattered radiation effects are removed without blurring edges, which is essential for surface detection (see Figure 4).

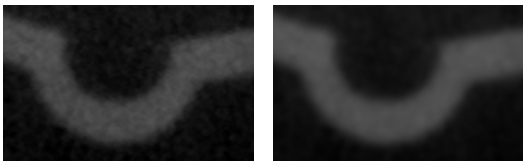

(a) (b)

Figure 4: Anisotropic-diffusion filter, axial cross section through a cutout of a 400V connector, before (a) and after anisotropic diffusion filtering (b). Smaller artefacts are removed and the dataset's noise is decreased.

3.2 Registration

When measuring a specimen using different X-Ray source setups of the CT scanner, slight changes in the

positioning and the orientation of the specimen in the dataset may occur. To avoid the propagation of this error, a registration procedure has to be carried out. In the DECT workflow the high energetic (HE) dataset is considered as the fixed image, as it is robust to artefacts. The low energetic (LE) dataset is considered as the moving image which is registered to the fixed image. In order to improve the performance of a registration algorithm concerning speed and exactness a multiresolution approach is commonly used. The fixed image and the moving image are decomposed into image pyramids, which downsample the image level by level. Starting at the top level of the pyramids the most coarse images of the two pyramids are registered to each other. Proceeding with the succeeding levels the registration is refined at each level. This guarantees a high robustness of the registration procedure.

Due to the different imaging modalities, a mutual information approach is used. To compute the mutual information between the fixed (HE) and the moving image (LE) the method of Mattes et al. [14], [13] is taken. This method evaluates the marginal and joint probability density function (PDF) at discrete positions (bins) which are uniformly spread within the dynamic range of the images. The entropy values are calculated by summing over the bins. Using this approach the fixed image PDF does not need to be smooth, because it does not contribute to the derivatives. A zero order (box car) B-Spline kernel is used for the fixed image intensity PDF. To ensure smoothness, the moving image intensity PDF is computed with a third order B-Spline kernel.

3.3 DECT fusion

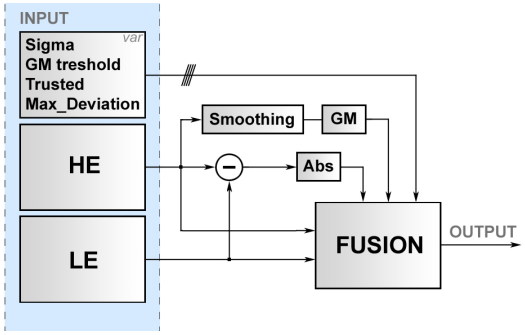

Figure 5: Principle of DECT fusion: The fusion of the LE and the HE input is performed at edge regions of the HE dataset. According to the amplitude of the gradient magnitude (GM) the fusion is linearly weighted. The absolute value difference image between LE and HE is used as a constraint to prevent from fusing artefacts.

The severe artefacts in the low energetic dataset (LE) change their characteristic and orientation according to measurement parameters and positioning of the specimen in the X-Ray beam. Common image fusion methods turned out to be inefficient and unsuccessful. Therefore we developed a DECT specific approach for image fusion (see Figure 5). In order to detect artefact affected regions an absolute value difference image between the HE and the LE measurements is computed. The difference image shows greyvalue inhomogeneities between the measurements and it is used as constraint for the use of LE data. As the main object structure is depicted best in the HE dataset, only the edges have to be improved with information from the LE dataset. So the HE dataset is smoothed using a gaussian filter kernel with a user defined *sigma* in order to extract a low noise gradient magnitude image with smooth edges. The resulting image contains all the regions to be enhanced by the LE dataset. Subsequently the datasets are combined by arithmetic image fusion, which is linearly weighted according to the gradient magnitude at a specific position starting at a user defined *GM_threshold*. The higher the gradient magnitude is at a certain position, the higher is the weight of the LE dataset and the lower is the weight of the HE dataset. The constraint of the absolute values difference image limited by *max_deviation* serves as a reduction factor for the LE dataset's weight. A high value in the difference image indicates an area where the LE data contains servere artefacts (e.g. streaks) and that the LE dataset is less reliable. Furthermore, for trusted regions of hardly any difference in the greyvalues of the LE and the HE data, a *trusted* level is defined, which weights the LE dataset with 100%. For the effect of arithmetic image fusion see Figure 4.

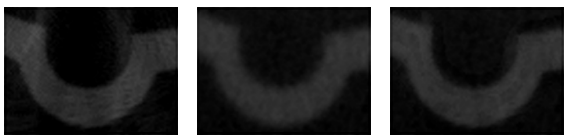

(a) (b) (c)

Figure 6: Axial cross section through a cutout of a 400V connector. LE image (a), HE image (b) and fused image (c). Using our image fusion approach the edges are significantly enhanced for surface extraction without adopting artefacts of the LE dataset.

3.4 Local surface extraction

In order to additionally improve the surface mesh, a local approach is used [22]. First a reliable global iso-

surface of the fused dataset is extracted, which contains the topology of the underlying data but still contains inhomogeneities and errors due to the local varying characteristics of the greyvalues. To correct these misclassifications, each surface vertex is moved in the direction of the surface normal. The vertex location is moved along the normal where the gradient magnitude reaches its maximum. This is accomplished by trilinear interpolation of the greyvalues along the surface normal and computing the derivative of the generated greyvalue profile. As a constraint, a user-defined maximal deviation for the repositioning of a vertex is used. The local modification of vertices with predefined constrains supports in generating a surface model with improved precision. To reduce repositioning failures due to noise, not only the density profile along the normal is taken into account, but also close-by profiles along directions parallel to the normal. In the tangent plane to the normal direction, a 3*3 neighborhood is used to compute 9 density profiles (see Figure 7). The directional derivative along each profile is estimated according to $f'(\mathbf{x}) = f(\mathbf{x}) - f(\mathbf{x}-1)$, where $\mathbf{x}$ and $\mathbf{x}-1$ are successive positions along the profile. For each of the nine profiles the position with the maximal gradient is determined. The improved edge location is calculated by using either the weighted mean of all positions according to the weighting matrix $\begin{pmatrix} 1 & 2 & 1 \\ 2 & 4 & 2 \\ 1 & 2 & 1 \end{pmatrix}$ or the median position is taken.

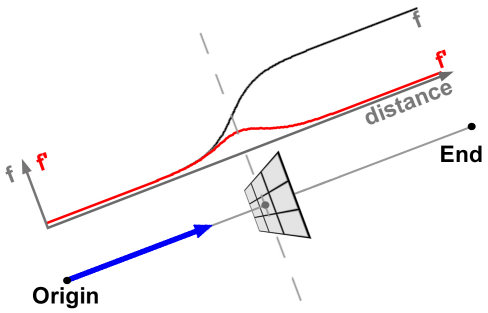

Figure 7: Local surface extraction adapts the surface model by moving surface vertices in the direction of the corresponding point normal to a position of the maximum gradient magnitude. The dataset's noise is reduced by considering the neighborhood of a surface point candidate.

4 Results and discussion

In this section results are discussed when applying the DECT workflow for surface extraction from multi-material components in different industrial parts. For all parts the high absorbing material is covered by low absorbing material. All CT scans were performed on a HWM RayScan 250E system with a 225 kV micro-focus and a 450 kV macro-focus X-Ray source. For the micro-focus setup the best achievable resolution is 7 μm/voxel depending on the maximum dimension of the specimen. Using the macro-focus setup the best achievable resolution is 150 μm/voxel which is again constrained by the diameter of the probe. Reference measurements were performed on a Zeiss SPECTRUM 700 (ST3/RDS-RST) Vast XXT coordinate measuring machine with a longitudinal error of measurement of 2.2 μm $\cdot \frac{l}{300}$ (where l is the length of the measured specimen) . Our demo application was implemented in Visual C++ using ITK [6] for image processing and VTK [20] for visualization. All 3D views are rendered using raycasting. For evaluation of deviations the commercial software systems Raindrop Geomagic Qualify 7 [18] and Carl Zeiss Calypso [26] with CT expansion are used.

4.1 Specimens

4.1.1 Polyethylene testpart

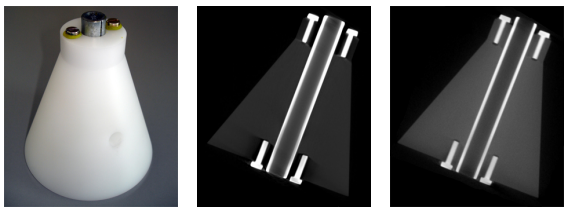

(a) (b) (c)

Figure 8: Specimen one: The left image shows a photograph of the PE testpart (a). The axial cross section of micro-CT scan (b) shows severe artefacts in the area of the metallic screws which are depicted by the dark areas around the screws. Image (c) Shows the cross section of the macro-CT scan. The HE scan is less artefact affected by not as precise as the LE dataset.

Specimen one (Figure 8) is a homogeneous polyethylene (PE) testpart used for analysis of parameter variations in dimensional measurement. The PE testpart consists of a cone with an attached cylinder. Several drill holes all over the specimen are serving to determine the exactness of a scan by evaluating distances and dimensions of the holes. In the base of the specimen four smaller drill holes are placed, as well as two drill holes on the top. Furthermore there are a major central drill

and a drill hole from the surface of the cone to the center of the specimen. A steel round bar is placed in the major central drill and steel screws are placed and fixed in the drill holes, which makes this part a multi-material object. Specimen one was measured twice without moving the specimen but using different X-Ray setups. The first measurement was a high energetic (HE) macro-focus scan in order to determine the structure of the specimen. The second measurement was a low energetic (LE) high precision micro-focus scan. For artefact reduction purposes, the X-Ray spectrum is hardened by using pre-filtering plates. All datasets are stored in 16 Bit unsigned short. For detailed CT measurement parameters see Table 1.

Table 1: Parameters for specimen one

Parameter	Specimen one HE	Specimen one LE
projections	900	900
voltage (kV)	440	200
current (μA)	1300	450
integration time (ms)	2000	1000
pre-filtering	1 mm W + 1.5mm Cu	1mm Cu
datasize	508*523*611	508*523*611
voxelsize (μm)	200	200

4.1.2 400 Volt connector

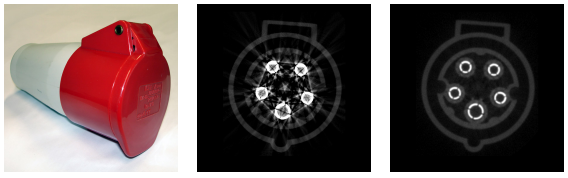

(a) (b) (c)

Figure 9: Specimen two: The left image shows a photograph of the power connector (a). The axial cross section of the low energetic micro-CT scan (b) shows the typical characteristic of artefacts within multi-material components due to too low X-Ray energies: Starting from the pins severe streaking artefacts can be found. Using the high energetic macro-CT scan, most of the streaking artefacts can be removed (c).

Specimen two (Figure 9) is a 400 Volt power connector according to European IEC 60309 system. This component consists of a plastic housing, the five pins, two steel-screws to connect the housing parts, two steel-screws for the strain relief of the power cable, a spring and a bearing for the cap mechanism. Figure 2 shows a 3D rendering of a typical micro-focus CT scan. This specimen shows severe artefacts around the power pins. Greyvalue modifications due to scattered radiation of the metal components are exceeding the plastic's greyvalue. CT Measurement parameters are listed in Table 2.

Table 2: Parameters for specimen two

Parameter	Specimen two HE	Specimen two LE
projections	1080	1440
voltage (kV)	440	210
current (μA)	1000	680
integration time (ms)	1000	1000
pre-filtering	1 mm W + 1.5 mm Cu	2 mm Cu
datasize	391*552*847	391*552*847
voxelsize (μm)	171	171

4.1.3 Terminal block

(a) (b) (c)

Figure 10: Specimen three: Photograph of the terminal block (a). In the cross section of the micro-CT scan (b) streaking artefacts around the metallic clamps are present. The loss in contrast can be seen when using lower X-Ray energies. In the area of the screws the disadvantages of the macro-focus CT are revealed: Fine structures disappear (c).

Specimen three (see Figure 10) is a terminal block from home automation systems. Terminal blocks provide convenient means of connecting electrical wires and are widely used. This part is built up using a plastic body, which supports as carrier of the metal clamps, a spring, which fixes the terminal on the top hat rail, and finally the two metal clamps holding the wires, which are connected by the power rail. This test object was chosen because of its regular structure and a convenient geometry for coordinate measurement technology. In total 16 random inspection features of the object were specified to calculate the dimensional deviation between the different measuring modalities and a reference model. The CT measurement parameters for the terminal block are listed in Table 3. A high precision reference measurement was carried out using a coordinate measuring machine.

Table 3: Parameters for specimen three

Parameter	Specimen three HE	Specimen three LE
projections	1080	1080
voltage (kV)	400	160
current (μA)	2200	660
integration time (ms)	1000	2000
pre-filtering	1 mm W + 1.5 mm Cu	2 mm Cu
datasize	88*322*324	88*322*324
voxelsize (μm)	200	200

4.2 Tuning the DECT workflow

General guidelines for tuning the DECT workflow are discussed in the following section. To produce reliable surface models for dimensional measurement, the parameter settings of each step is essential. As prefiltering step an anisotropic diffusion filter (Figure 3a) is used, which creates a more homogeneous dataset without modifying edge information. Especially for the LE dataset this step is crucial in order to reduce noise and smaller artefacts. The aim of prefiltering is to improve the information to be fused. The noisier a dataset is, the more iterations of the diffusion filter have to be applied. The conductance C (equation 3) controls the local degree of smoothing and the areas to be smoothed. The higher the conductance, the more the diffusion filter acts like an isotropic filter, smoothing all regions. The smaller the conductance, the more features are preserved. As we do not want to preserve artefacts a rather high setting of the conductance is used for the LE dataset and a even higher setting for the HE dataset. For the LE dataset, a parameter setting of 5 iterations and a conductance of 10-50 turned out to produce reliable results. For the HE measurement we used 10 iterations at a slightly higher conductance of 75 to compute a smoother dataset.

In the registration step (Figure 3b), the method of Mattes et al. [14] is applied, using the HE dataset as fixed image and the LE dataset as moving image. For the image pyramides a fixed setting of five levels is used.

For the DECT image fusion part (Figure 3c) the gradient image of the Gaussian smoothed HE datasets determines the image fusion regions. The bigger these regions are, the smoother the image fusion will adopt features of the LE dataset. Using a sigma value of at least 0.2, a blurry image of the HE dataset is generated. When applying a gradient magnitude filter on this input image, a smooth gradient image is computed. Depending on the dataset and the quality of edges, an edge image is produced with a smooth increase and decrease of the gradient magnitudes. The width of a typical edge is supposed to be approximately 5 to 10 voxels wide for a smooth image fusion. The trusted level which weights the LE dataset with 100% should not exceed the standard deviation of the HE dataset. Otherwise artefacts are transferred to the resulting image.

In the local surface extraction step (Figure 3d) a reliable surface model is extracted using a global threshold. For the locally improved surface mesh evaluating the maximum position of the gradient magnitude profile along the surface model, the number of samples and the maximum sample distance have to be specified. The finer the sampling rate, the finer the positioning of the surface vertices. Generally a setting of 50 samples for each voxel is a valuable compromise between computation time and accuracy. A more difficult parameter is the maximum sample distance, which serves as a constraint for the repositioning of vertices. Exceeding a maximum sample distance of 5 times the voxelsize may produce erroneous results due to erroneously oriented surface normals of the isosurface. So usually settings of 2 to 5 times the voxelsize produce a reliable improved surface mesh. Finally the normal direction (positive, negative or both directions) is a parameter to be set. Due to noise in the surface mesh considering both directions produces the most reliable results.

4.3 Evaluation of DECT workflow results

To get an overview of deformations throughout the whole component, variance comparisons are widely used. The primary usage of variance comparisons is to compare the measured geometry of a specimen with reference geometry data, e.g. of a CAD model. A common visualization method for variance comparison is color coding the reference's surface corresponding to the local deviation. To show the different results of generating surface models, variance comparisons between the CAD model and three surfaces are depicted. The first surface is due to the best global threshold from the LE data. The second surface is due to the best global threshold from the HE data. The third surface is the result of our proposed DECT workflow result. Note: the CAD model does not contain the data of the screws and the round bar. The best global thresholds are empirically determined. The metal parts are equipped to show the loss in data quality when placing high absorbing components within low absorbing components. This produces deformations due to artefacts when extracting an isosurface. In Figure 11a high deviations due to streaking artefacts and scattered radiation are depicted in dark red and dark blue. In less artefact affected areas, a high correspondence between the CAD model and LE measurement can be seen. Figure 11b shows a more ho-

mogeneous distribution of deviations. For the HE measurement, the mean deviation is higher but hardly any artefacts affect the surface. Applying the DECT workflow the advantages of both measurements can be combined. The variance comparison shows higher accuracy than the HE dataset without introducing artefacts of the LE dataset (see Figure 11c).

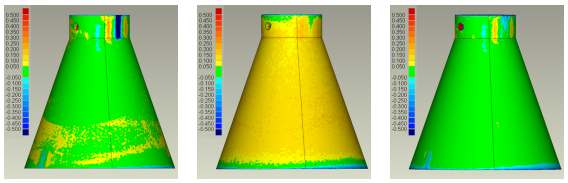

(a) (b) (c)

Figure 11: Variance comparison of specimen one between CAD model and extracted surface models. Deviations are colorcoded using the same scale. Figure (a) shows the variance comparison using a global threshold applied on the LE dataset and in Figure (b) on the HE dataset. The result when applying the DECT workflow on specimen one is depicted in (c). Artefacts of the LE measurement can be avoided to a high extent. The smoother characteristics of the DECT surface is indicated by the large low deviation area (green).

Specimen two was chosen to demonstrate our DECT workflow's ability to produce reliable surface models without holes. The multi-material characteristics of this specimen produce streaking artefacts and scattered radiation in the reconstructed dataset. These circumstances are depicted in Figure 2 and 9. When extracting an isosurface from the LE dataset, common methods like Otsu's method [16] turned out to produce unusable results. The best global threshold to create a surface model was determined again empirically. However, a complete and reliable measurement is impossible due to severe artefacts of the derived surface model (Figure 12a). Using the HE dataset of specimen two, a reliable surface model may be extracted but due to the larger focal spot of the macro-focus source fine details get lost. Furthermore due to the much higher ambient noise level of the HE dataset, the generated surface model has a rather coarse surface structure (see Figure 12b). When applying the DECT workflow, part of the details are reconstructed by incorporating details from the LE dataset. In the resulting surface model holes were removed, surface deformations through scattered radiation were avoided and fine details were fused into the resulting dataset (see Figure 12c).

Dimensional measurement accuracies are verified by specification and evaluation of 16 inspection features (3

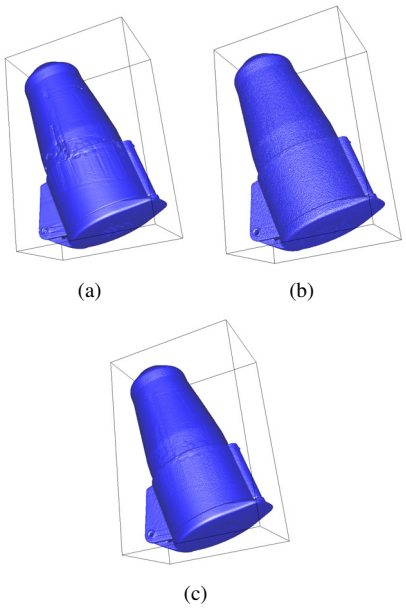

(a) (b) (c)

Figure 12: Surface extraction of specimen two using a global threshold applied on the LE dataset (a) and on the HE dataset (b). The result when applying the DECT workflow on specimen two is depicted in (c). Artefacts of the LE measurement can be avoided. The coarse structure and the higher mean deviation of the HE measurement was significantly reduced. DECT fusion even preserves fine details like the sticker on the jacket of the 400 V connector.

diameters of cylinders and 13 distances). As reference, specimen three was measured using a high precision coordinate measuring machine. In order to point out the differences in dimensional measurement, the same features were evaluated in the LE measurement, the HE measurement and the resulting dataset of the DECT workflow using CT-Calypso. Using this tool inspection features can be evaluated in the volumetric dataset as well as in surface models. In Figure 13 a diagram of the measurement inaccuracies was plotted: On the Y axis the mean deviation per inspection feature in % is depicted. On the X axis the different measurement modalities and the output of the DECT workflow are depicted. As expected, the LE measurement produces a result with higher precision than the HE measurement. In comparison to the LE dataset the HE measurement is less artefact affected. Applying the DECT workflow, artefacts are reduced, which can be seen in the lower mean deviation per inspection feature (see Figure 13). For specimen three the mean deviation per inspection feature can be lowered from 0.31% of the HE dataset and 0.25% of the LE dataset to 0.16% for the DECT workflow.

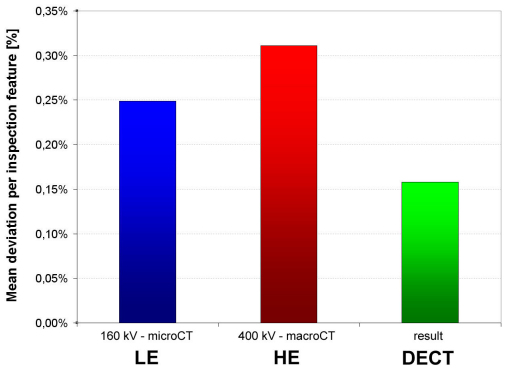

Figure 13: Evaluation of 16 inspection features of specimen three. The mean deviation per inspection feature in % was plotted over the different measurement modalities: LE, HE and DECT workflow. The DECT fusion of details from the LE dataset is used to improve accuracy without adopting artefacts.

5 Summary and conclusions

A novel pipeline for dimensional measurement of multi-material industrial components is presented, allowing reproducible and robust surface extraction. The introduced DECT workflow exploits a dual source / dual exposure approach of dual energy computed tomography. It facilitates dimensional measurement of artefact affected datasets from multi-material components. Several algorithms are extended to take the two data sources of micro- and macro-CT with complementary strengths and weaknesses into account. A specific fusion algorithm has been developed to integrate the accuracy of LE data with the robustness of the HE data. In the analysis section the accuracy and the applicability of the DECT workflow on industrial components has been discussed. In case of the PE testpart (specimen one) variance comparisons were shown to depict the improved quality of the fused dataset. The applicability of the DECT workflow for creating smooth and closed surfaces was depicted for a real world industrial component: the 400 Volt power connector. For the terminal block, the mean deviation per inspection feature over 16 inspection features could be decreased from 0.31% of the HE dataset and 0.25% of the LE dataset to 0.16% for the DECT workflow result.

A major aim of our future work is to further improve the quality of image fusion. Furthermore measuring the specimens at different resolutions and registering the datasets in order to exploit the different imaging modalities will also be a topic of our future work.

Acknowledgements

The presented work has been funded by the FH-Plus project ”Zerstörungsfreie und In-situ-Charakterisierung von Werkstücken und Materialien unter besonderer Berücksichtigung von Brennstoffzellen” (see http://www.fh-wels.at and http://www.3dct.at) of the Austrian Research Promotion Agency (FFG). Furthermore this work is partly supported by the PVG project, Austrian Science Fund (FWF) grant no P18547. Thanks to the vis-group of the Vienna University of Technology, Institute of Computer Graphics and Algorithms, for support in designing this method and especially M. Reiter, E. Schlotthauer, D. Salaberger and the CT group of the Upper Austrian University of Applied Sciences - Wels Campus for CT measurements, reference measurements, illustrations and fruitful discussions when evaluating this method.

References

[1] S. Bischoff and L. Kobbelt. Isosurface reconstruction with topology control. In *Pacific Conference on Computer Graphics and Applications*, pages 246–255, 2002.

[2] S. F. Gibson. Constrained elastic surface nets: generating smooth surfaces from binary segmented data. In *Lecture Notes In Computer Science*, volume 1496, pages 888–898, 1998.

[3] C. Heinzl, R. Klingesberger, J. Kastner, and E. Gröller. Robust surface detection for variance comparison. In *Proceedings of Eurographics/IEEE-VGTC Symposium on Visualisation*, 2006.

[4] J. Hsieh. *Computed Tomography: Principles, Design, Artifacts and Recent Advances*. SPIE-The International Society for Optical Engineering, 2003.

[5] R. Huang, K.-L. Ma, P. McCormick, and W. Ward. Visualizing industrial CT volume data for nondestructive testing applications. In *VIS ’03: Proceedings of the 14th IEEE Visualization 2003 (VIS’03)*, page 72, 2003.

[6] L. Ibanez and W. Schroeder. *The ITK Software Guide*. Kitware, Inc., 2003.

[7] M. Iovea, O. Duliu, G. Oaie, C. Ricman, and G. Mateiasi. Dual-energy computer tomography and digital radiography investigation of organic

and inorganic materials. In *Proceedings of European Conference on Non Destructive Testing*, 2006.

[8] M. Iovea, G. Oaie, C. Ricman, G. Mateiasi, M. Neagu, S. Szobotka, and O. Duliu. Dual energy x-ray computer axial tomography and digital radiography investigation of cores and other objects of geological interest. In *32nd International Geological Congress*, 2005.

[9] S. Kasperl. *Qualitätsverbesserungen durch referenzfreie Artefaktreduzierung und Oberflächennormierung in der industriellen 3D-Computertomographie*. PhD thesis, Technische Fakultät der Universität Erlangen Nürnberg, 2005.

[10] J. Kastner, E. Schlotthauer, P. Burgholzer, and D. Stifter. Comparison of x-ray computed tomography and optical coherence tomography for characterisation of glass-fibre polymer matrix composites. In *Proceedings of World Conference on Non Destructive Testing*, pages 71–79, 2004.

[11] J. J. Lewis, R. J. OCallaghan, S. G. Nikolov, D. R. Bull, and C. N. Canagarajah. Region-based image fusion using complex wavelets. In *7th International Conference on Information Fusion*, 2004.

[12] W. Lorensen and H. Cline. Marching cubes: A high resolution 3D surface construction algorithm. In *ACM SIGGRAPH Computer Graphics*, volume 21, pages 163–169, 1987.

[13] D. Mattes, D. R. Haynor, H. Vesselle, T. Lewellen, and W. Eubank. Nonrigid multimodality image registration. In *Medical Imaging 2001: Image Processing*, pages 1609–1620, 2001.

[14] D. Mattes, D. R. Haynor, H. Vesselle, T. Lewellen, and W. Eubank. PET-CT image registration in the chest using free-form deformations. In *IEEE Transactions in Medical Imaging*, volume 22, pages 120–128, 2003.

[15] D. Mueller, A. Maeder, and P. O'Shea. The generalised image fusion toolkit (gift). In *IJ - 2006 MICCAI Open Science Workshop*, 2006.

[16] N. Otsu. A threshold selection method from grey level histograms. In *IEEE Transactions on Systems, Man, and Cybernetics*, volume 9, 1979.

[17] P. Perona and J. Malik. Scale-space and edge detection using anisotropic diffusion. In *IEEE Transactions on Pattern Analysis and Machine Intelligence*, volume 12, pages 629–639, 1990.

[18] Raindrop. Raindrop: The magic of making it simple. Raindrop Geomagic: WWW: http: // www.geomagic.com /, 18th March 2007.

[19] V. Rebuffel and J.-M. Dinten. Dual-energy x-ray imaging: Benefits and limits. In *Proceedings of European Conference on Non Destructive Testing*, 2006.

[20] W. Schroeder, K. Martin, and B. Lorensen. *The Visualization Toolkit*. Kitware, Inc., 2004.

[21] Siemens. Dual source CT. Siemens-Healthcare: WWW: http: // healthcare.siemens.com / ct_applications / dualsource / somatom / index6.html, 18th March 2007.

[22] H. Steinbeiss. *Dimensionelles Messen mit Mikro-Computertomographie*. PhD thesis, Technische Universität München, 2005.

[23] VolumeGraphics. *VG Studio Max 1.2 - User's Manual*. 2004.

[24] R. T. Whitaker and D. E. Breen. Level-set models for the deformation of solid objects. In *The third international workshop on implicit surfaces*, pages 19–35, 1998.

[25] Wikipedia. Metrology. Wikipedia: WWW: http: // en.wikipedia.org / wiki / Metrology, 18th March 2007.

[26] C. Zeiss. Calypso - visual metrology. Carl Zeiss - Industrielle Messtechnik: WWW: http: // www.zeiss.de / calypso, 18th March 2007.